Classification of Stratosphere Winter Evolutions Into Four Different Scenarios in the Northern Hemisphere

Alexis Mariaccia, Philippe Keckhut, Alain Hauchecorne

Author Contributions:

Conceptualization: A. Mariaccia
Investigation: A. Mariaccia, P. Keckhut
Methodology: A. Mariaccia, P. Keckhut, A. Hauchecorne
Project Administration: P. Keckhut, A. Hauchecorne
Software: A. Mariaccia
Supervision: P. Keckhut, A. Hauchecorne
Validation: P. Keckhut, A. Hauchecorne
Visualization: A. Mariaccia
Writing – original draft: A. Mariaccia

Classification of Stratosphere Winter Evolutions Into Four Different Scenarios in the Northern Hemisphere

A. Mariaccia[1] , **P. Keckhut[1]** , **and A. Hauchecorne[1]**

[1]Laboratoire Atmosphères, Milieux, Observations Spatiales, UMR 8190, Institut Pierre-Simon Laplace, Université Versailles-Saint Quentin, Université Paris-Saclay, Guyancourt, France

Abstract Among the 70 northern hemisphere winters from 1950 to 2020, 61 have been classified into four independent scenarios with a new technique based on analyzing empirical orthogonal functions of stratospheric zonal wind fluctuation patterns at the edge of the polar vortex. These four scenarios represent a typical zonal wind evolution in the stratosphere modulated by timings of stratospheric warmings occurring in winter. First, there are three scenarios (January mode, February mode, and Double mode) for which the polar vortex generally breaks down with a reversing of zonal winds in midwinter, known as sudden stratospheric warmings (SSWs) events, at different times. The last one is a non-perturbed scenario with two under-modes for which only the timing of the polar vortex transition to its summer state differs, either radiative or dynamical. Consistently with these wind patterns, the wave-1 and wave-2 anomaly evolutions confirm that these scenarios are associated with independent dynamics behaviors and significant differences between wave-1 and wave-2 activities. We found that the wave-1 anomaly evolutions drop systematically for each scenario when the stratospheric winds weaken, while this correlation with the wave-2 anomaly evolutions is not observed for all scenarios. These different dynamical behaviors confirm that the scenarios are either mainly dynamically driven by wave-1 or both driven by wave-1 and wave-2. Until early December, the modes possess similar increasing evolutions of the wave-1 activity due to the seasonal cycle. After, the scenarios separate, suggesting that the mechanisms responsible for the winter unfolding act in the previous months.

1. Introduction

Each year in both hemispheres, when the summer is finishing, a cold polar vortex with westerly winds forms in the stratosphere as the incoming solar radiation decreases. During its radiative life cycle, stratospheric warmings affect the position and the structure of the polar vortex leading to a vortex breakdown and the reversing of the westerly winds for the most extreme cases (Baldwin et al., 2021), the so-called sudden stratospheric warmings (SSWs) events observed for the first time by Scherhag (1952). Then, with the arrival of the following spring, this vortex weakens and decays when the winds return to their easterly summer state. Since their discovery, much evidence has shown that SSWs impact afterward the tropospheric circulation confirming the existence of the two-way stratospheric-tropospheric dynamical coupling (Baldwin & Dunkerton, 2001; Labitzke, 1981; Thompson & Wallace, 2001).

Indeed, the birth mechanism of SSWs, according to the models developed by Matsuno (1971) and Andrews et al. (1987), implies an interaction between the mean flow and upward propagating planetary waves from the troposphere to the stratosphere. However, as sources of planetary waves are mainly the orography or the high-temperature gradient between ocean and land, nearly all observed SSWs occurred in the Northern Hemisphere (NH). In contrast, the polar vortex in the Southern Hemisphere (SH) generally remains very strong in wintertime due to the small amplitude of planetary waves. Although one exception with a major SSW can be raised during the SH spring of 2002 (Charlton et al., 2005; Krüger et al., 2005). While in the NH, major SSWs, on average, occur about six times per decade (Charlton & Polvani, 2007) with a substantial variability over decades (Domeisen, 2019).

Since SSWs are observed and studied, the scientific community has been searching to classify them according to several physical criteria illustrating their impact on the evolution of the polar vortex. Over the years, only the following classification of SSWs into four categories referring to their magnitude and timing has remained widely used: Major, Minor, Final, and Canadian warmings. However, still, nowadays, no clear definition for these four SSW types exists, resulting in different classifications among the studies (Butler et al., 2017).

Initially based on the rising of the temperature within the vortex by the World Meteorological Organization (WMO) for the International Years of the Quiet Sun in 1964, the definitions of major SSWs given in the literature have evolved and are now almost exclusively defined according to the reversal from westerly to easterly of the stratospheric zonal winds at the edge of the vortex (Butler et al., 2015). These current definitions include the distinction between major SSWs and final stratospheric warmings (FSWs) corresponding to the last inversion of the climatological winter westerlies to summer easterlies in the stratosphere. Similarly, the definition of minor SSWs is now based on a strong stratospheric wind deceleration without reversing the polar winds (e.g., Maury et al., 2016). Finally, there is still no consensus on the classification of Canadian warmings (warming occurring in early winter with an eastward shift of the Aleutian high), that is, whether or not they must be differentiated from major SSWs when winds reverse (Butler et al., 2015).

For many years, the attention has been focused primarily on major SSWs as they substantially impact the polar vortex and the weather in the troposphere. Indeed, numerous tentative classifications of major SSWs have been explored according to different criteria. For instance, Charlton and Polvani (2007) (hereafter CP07) introduced a classification of major SSWs based on the vortex geometry, that is, the vortex is either displaced off of the pole or split into two distinct vortices. It has been found that split events occur mainly in January and February, and displaced events occur mainly in December and March. Mitchell et al. (2013), who improved the classification technique developed by CP07, concluded that displacements and splitting vortex events later influence the tropospheric weather differently.

Other studies have attempted to classify major SSWs according to their low impact, and the tropospheric response (Charlton-Perez et al., 2018; Domeisen, 2019; Kodera et al., 2016). However, the occurrence of major SSWs limits these classifications since they overlooked the minor SSWs, occurring more frequently during winters and weakening the vortex significantly but without reversing the winds (Maury et al., 2016), preventing, in fine, a complete understanding of the mean stratospheric changes. The advantage of this study is that the classification is based on the winter evolutions and not on the SSW type in mid-winter, and therefore no winters are discarded.

Regarding FSWs, on the other hand, a criterion based on their timing of occurrence has generally been used to classify them into "early" or "late" events (Waugh & Rong, 2002). In the NH, the generation of early FSWs is similar to the one for SSWs events, which tend to be also wave-driven (Vargin et al., 2020). In contrast, late FSW events are more radiatively-driven as the polar vortex weakens with the increase of incoming solar radiation. Recently, Butler and Domeisen (2021), who undertook a new classification of FSWs according to the dominant wave geometry prior to reversing the winter westerlies in both hemispheres, have found that wave-1 events tend to shift the polar vortex toward Eurasia in the NH. In contrast, wave-2 events are the precursor of an elongated or split vortex over Canada and eastern Asia. Hauchecorne et al. (2022), in addition to their new classification of FSWs from 1950 to 2020 according to their nature and their occurrence, either "dynamical" or "radiative" events, investigated the seasonal memory of the stratosphere. They found that the polar vortex on a given month is anti-correlated with its state 2–3 months earlier and that the stratosphere keeps a memory of its state of April–May until at least July.

This work aims to improve our overall understanding of the handling of winters by investigating principal winter typologies and inferring how the early winter is related to the mid-winter and then how the mid-winter influences the early spring. The novelty here is that we pursue the investigation of the stratosphere memory initiated by Hauchecorne et al. (2022) over the same period with a new technique of classification of winters based on the principal component analysis of the evolution of the polar vortex. To our knowledge, it is the first time that this type of classification has been undertaken and, in addition, by using the new ERA-5 reanalyzes of wind at 10 hPa-60°N produced by the European Center for Medium-Range Weather Forecasts (ECMWF). The other solid motivation for this new classification is its usefulness for improving the models' weather prediction in the stratosphere.

This paper is organized as follows: A detailed description of the data used as well as an illustration of the wave contributions (wave-1 and wave-2) to the vortex geometry during two SSWs are given in the next section. Then, the distribution of major and important SSWs (ISSWs) and FSWs is shown and discussed in Section 3. The method and the result of the classification are presented in Section 4. In Section 5, a more detailed characterization of each scenario is done. The mean evolutions of the wave amplitudes for each scenario are presented and discussed in Section 6. Finally, a discussion and a conclusion are given in Section 7.

2. Data Description

Wind and geopotential data used here are extracted at 10 hPa-60°N for the 1950–2020 period from the final product of reanalyzes ERA-5 built by the ECMWF. The ERA-5 reanalysis package is constructed thanks to worldwide observations provided by multiple sources (satellites, radiosondes, aircraft, rocketsondes, and other surface observations), which are assimilated with a 4D Var system (Hersbach et al., 2020). This last generation of reanalyzes benefits the updated ECMWF Integrated Forecast System IFS 41r2, improved bias correction techniques, and a better model parametrization of convection and microphysics than in the last ERA-Interim package (Dee et al., 2011). The ERA-5 output is produced hourly on a global horizontal resolution of 31 km and 137 vertical levels extending from the surface to the level pressure of 0.01 hPa (approximately 80 km). The ERA-5 package covers a period from 1950 to the present, providing the most extended reanalyzes series. Furthermore, recent studies evaluating ERA-5 reanalyzes in the middle atmosphere have confirmed their accuracy in the stratosphere in wintertime. For instance, Marlton et al. (2021) have found a good thermal representation up to 3 hPa and, in addition, Mariaccia et al. (2022) have shown that the model reproduced the variability accurately in the upper stratosphere during winter.

Thus, for this study, we dispose of wind and geopotential reanalyzes at 10 hPa-60°N to form the 70 winters between 1950 and 2020. For the years between 2000 and 2006, reanalyzes are from the re-run ERA-5.1 correcting the cold bias of the temperature in the lower stratosphere observed in ERA-5 for this period (Simmons et al., 2020). The zonal mean zonal winds and the amplitudes of waves 1 and 2 are daily computed from 1 November to 1 June. Figure 1 shows zonal wind evolutions during two winters. Winter 1960/1961 illustrates an unperturbed winter case, that is, a strong polar vortex, finishing with an abrupt transition to easterly winds in March typical of a dynamical end. Butler and Domeisen (2021) classified the FSW of this winter as an "early" event of wave-1 type. While, winter 2017/2018 illustrates a perturbed winter case with a major SSW of wave-2 type (Rao et al., 2018) occurring in February and finishing mid-April with a slow transition to the summer mode characteristic of a radiative end.

The wave components are calculated from the Fourier Analysis of geopotential as described in Pawson and Kubitz (1996):

$$Z = \overline{Z} + \sum_{k=1}^{2} Z_k \cos k\left(\lambda - \delta_k^Z\right), \tag{1}$$

where the overline represents the zonal mean, and each zonal wavenumber k is defined by its amplitude Z_k and phase δ_k. Here the phase corresponds to the longitude (east) of the maximum and lies in the range (0, 360/k). Figure 2 illustrates the decomposition of the stratospheric geopotential field for two dates after a major SSW. As expected, the wave-1 dominates for the vortex displacement event in January 2012 while the wave-2 dominates for the vortex splitting event in February 2018.

3. Distribution of SSWs From 1950 to 2020

3.1. Identifying the Different Type of SSWs

3.1.1. Identification of Important SSWs

Most studies have focused on SSWs when wind reverses from westerly to easterly, the so-called major SSWs, as they strongly impact the vortex state. Nevertheless, their occurrence is about one every 2 years which limits the statistical study of their timing for a data set containing only 70 winters. Hence, to observe a temporal trend in the occurring of SSWs, it is necessary to add other SSWs that weak significantly the vortex without reversing winds, the so-called minor SSWs. As minor SSWs have stimulated a few interests, very few definitions based on objective criteria exist to classify these events. According to the WMO, a minor SSW is characterized by a substantial increase of temperature, at least 25° for 1 week or less at any stratospheric level in the winter hemisphere. However, this temperature criterion is ambiguous as another WMO report stated that major SSW has a temperature increase of at least 30° for the same period (Butler et al., 2015). Here, to keep a continuity with the major SSW definition, we used a new wind criterion based on the study of Maury et al. (2016) to select, in addition to major SSWs, the warmings which affect the vortex significantly without reversing the wind. For the
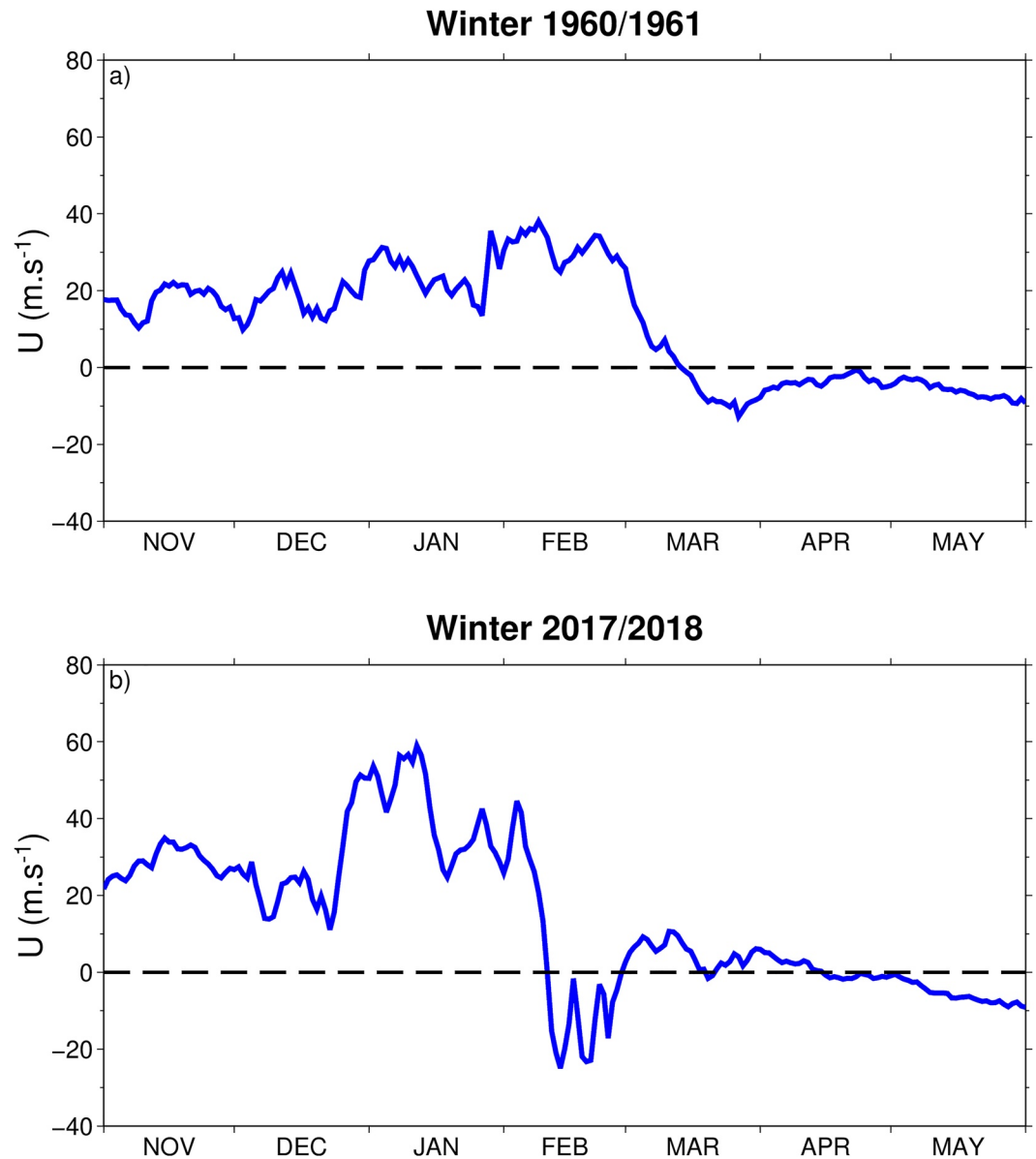
Figure 1. Evolution of zonal mean zonal wind (solid blue line) at 10 hPa-60°N for two winters illustrating a strong polar vortex finishing with an early and dynamical final stratospheric warming (FSW) of wave-1 type (a) and a polar vortex perturbed by a major sudden stratospheric warming of wave-2 type occurring in February and finishing with a late and radiative FSW (b).

remainder of this study, all these events will be referred to as the "ISSWs." The central date of each important SSW occurring during the 70 winters is determined as follows:

1. We search the first date d from which the zonal mean of zonal wind at 60°N-10 hPa falls below 10 ms^{-1}, threshold sufficient to detect events reducing significantly the planetary wave propagation and from which the vortex can be considered as weak (Maury et al., 2016).
2. From d, if u is not positive for at least 10 consecutive days before 30 April, the event is considered as an FSW event, and we stop to search other Important SSW. If not, the date d is saved as a central date of Important SSW.
3. Then, a 20-day mask is applied to avoid accounting twice the same event. At $d + 20$, if u is superior to 10 ms^{-1} the algorithm continues to search other event. However, in the case where u is still inferior to 10 ms^{-1}, we
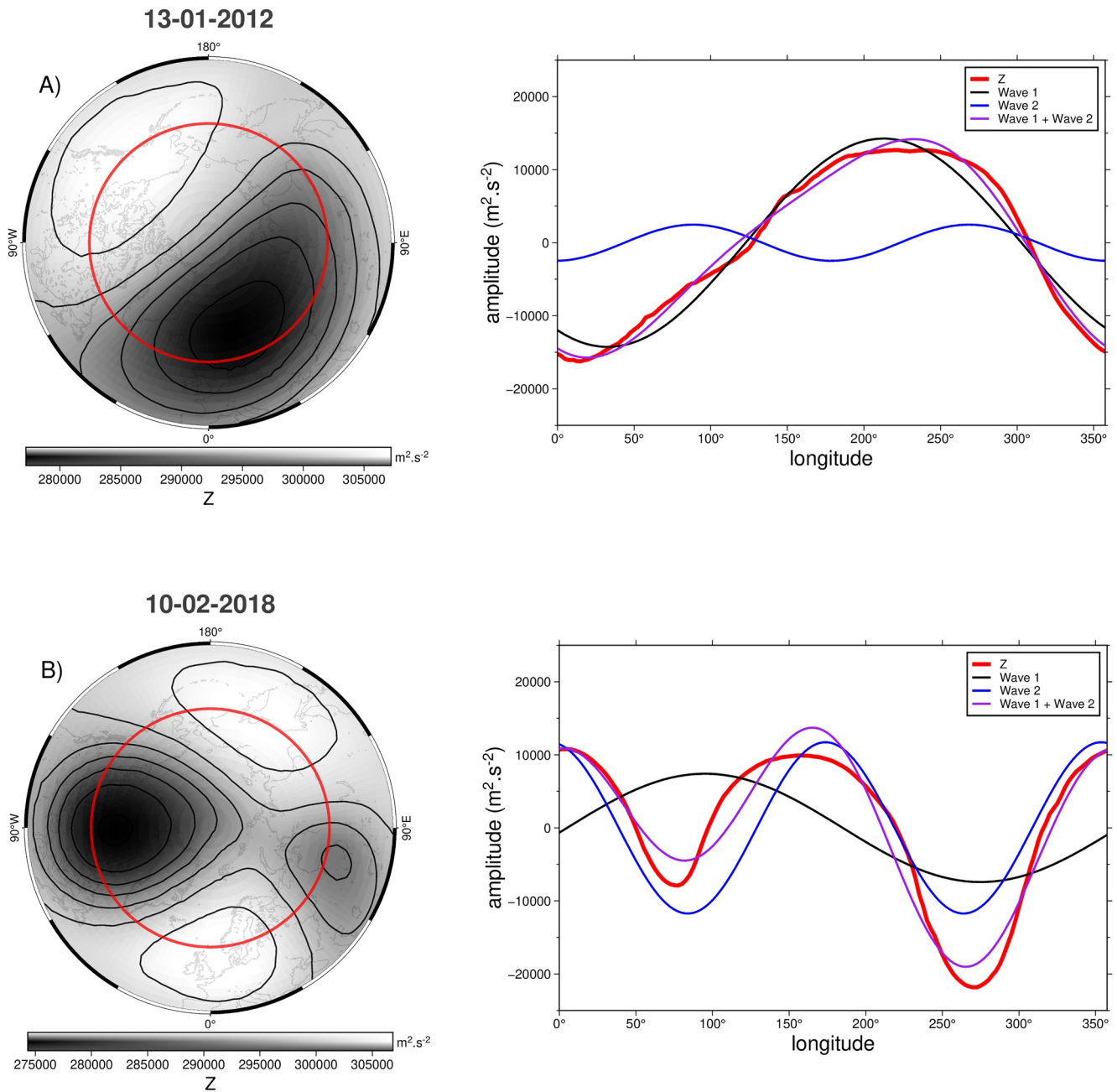
Figure 2. Geopotential contour at 10 hPa in the Northern Hemisphere for two dates showing two typical vortex evolutions (in black) after a sudden stratospheric warming: a displacement off of the pole (a) and a splitting into two vortices (b). The red circle is plotted on the 60°N and the geopotential evolution at this latitude is displayed on the right (red line). Contributions from wave-1 (black line) and wave-2 (blue line) to this geopotential are both displayed separately and together (purple line).

search the next date from which u is superior to 10 ms^{-1} and then the algorithm repeats the steps 1–3. If there is no date, the algorithm stops.

Here, we did not impose a warming duration, as performed in Maury et al. (2016) to separate minor from major SSWs, since only the ISSWs identification was needed for classifying afterward winters. With this algorithm, 105 important SSW events among the 70 winters have been detected, giving a ratio of 1.5 important SSW events per winter.

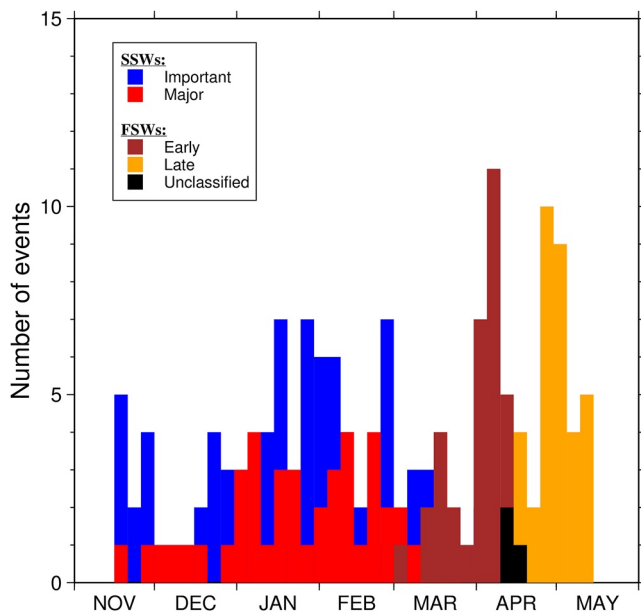**Figure 3.** Distribution of Important sudden stratospheric warmings (SSWs) (in blue), Major SSWs (in red) and final stratospheric warmings, in either "early" (in brown) or "late" (in orange) events and unclassified (in black), into intervals of 5 days from 1 November to 1 June from 1950 to 2020.

3.1.2. Identification of Major SSWs

The method used here to identify major SSWs is the same that proposed by Bancalá et al. (2012) which is based, as initiated by Charlton and Polvani (2007), on the zonal-mean zonal wind. The central date of the event is the day when the wind at 10 hPa-60°N reverses from westerly to easterly. Then, the algorithm searches the next day from which the wind becomes again westerly and then applies a 20-day mask. This interval, corresponding to the time necessary for the restoring of the polar vortex (Newman & Rosenfield, 1997), avoids to count several times the same event as the winds may oscillate around the 0 ms^{-1} value. In the case where the day after this interval of 20 days has easterly wind, then the algorithm searches the next day having westerly wind superior to 5 ms^{-1} to start again the searching for other major SSWs. Additionally, the algorithm searches the number of consecutive days of westerlies and the wind intensity following each event identified in order to detect if it corresponds to a FSW. Thus, an event is considered as a FSW whether the wind does not return to westerly for at least 10 consecutive days and that, among these days, the wind does not reach once 5 ms^{-1}. With this algorithm, 45 major SSWs have been detected among the 70 winters, which gives a ratio of 0.64 major SSW per year.

3.1.3. Identification of FSWs

However, the previous method developed by Bancalá et al. (2012) is not retained for FSWs identification as it subsists a winter for which none central date of FSW was computed. Thus, in order to have an FSW central date for each winter, the identification of FSWs is carried out with the same method employed by Butler and Domeisen (2021). This method is also based on the westerly winds reversal at 10 hPa-60°N, consistent with the definition of major SSWs used above. The central dates of FSWs are the first date before 30 June when u fall below 0 ms^{-1} and do not return to westerly for more than 10 consecutive days. As a result, the median date of the 70 FSWs identified is 15 April. As in Butler and Domeisen (2021), we classified afterward as "early" event FSWs occurring 2 days prior to the median date and as "late" events those occurring 2 days after the median date. These two FSW types are illustrated in Figure 1. With this algorithm, 33 winters have been classified as "early" events, 32 winters as "late" events, and five winters remain unclassified. Recently, Hauchecorne et al. (2022), who used a criterion based on temperature anomaly, have shown that FSWs are either "dynamical" and early (with a positive temperature anomaly superior to +10 K as for mid-winter SSWs) or "radiative" and late (with temperature anomaly inferior to 0 K). Their method found 20 winters with a radiative end and 20 winters with a dynamical end among the 70 winters from 1950 to 2020.

The comparison between these two classifications reveals, first, a perfect agreement for the 20 winters with a dynamical end which are all classified as "early" here, and second, that among the 20 winters with a radiative end, 18 winters are considered as "late" and two are unclassified. These two winters with unclassified FSWs (1988/1989 and 2017/2018) have both a late transition occurring mid-April (see Figure 1b) characteristic of winters having a radiative end. Moreover, Butler and Domeisen (2021), who studied FSWs from 1958 to 2019 in the NH, classified these both winters with a "late" FSW. Consequently, and to keep a consistency with the classification carried out by Hauchecorne et al. (2022), these two winters are considered as having a late and radiative end for the remaining of this study.

The occurrence distribution of major and important SSW events, as well as FSW events identified with these algorithms, is shown in Figure 3.

3.2. Discussion on SSWs and FSWs Distribution

As expected, major SSWs occur mainly during the mid-winter, in January and February (Figure 3), when the planetary wave activity is very strong (Fusco & Salby, 1999), causing the weakening and then the breakdown of the vortex. The major SSW distribution shows two peaks in January and February with nearly the same number of events. Similar preferred timings for major SSWs have been observed in other studies, such as in Limpasuvan
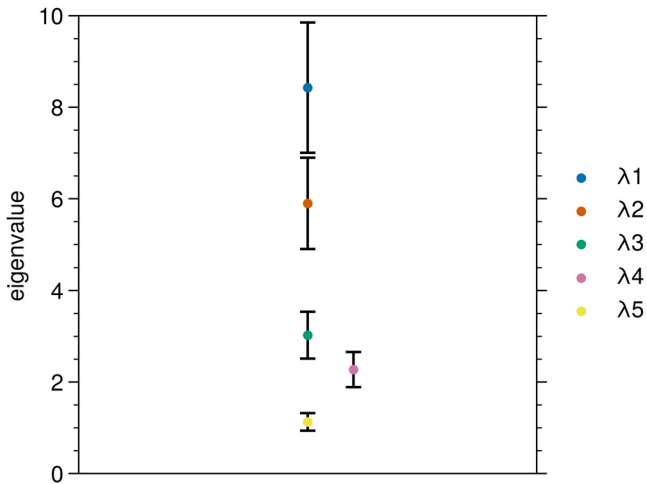
Figure 4. Schematic diagram of the first five eigenvalues λ_α associated with the first five empirical orthogonal function modes. The standard error for each eigenvalue, represented with the error bars, are computed with the North's "rule of thumb" for $N = 70$.

et al. ([2004](#)) who used 44 years of reanalyzes (1958–2001), suggesting that central dates of SSWs are not distributed randomly during winter. However, to our knowledge, none of them have been tempted to study this distribution as it is done here, that is, by searching how ISSWs' timings, illustrated by these peaks, influence afterward the winter evolutions. Thus, the major SSW distributions shown here constitute this study's first motivation to relate the preferential periods for which SSWs occur to a particular winter typology. However, despite these first trends observed, the number of major SSWs detected is insufficient to infer all the temporal trends in the occurrence of SSWs impacting the polar vortex significantly.

In order to complete and confirm the SSWs' timings, the distributions of ISSWs and FSWs are also studied. Indeed, the ISSWs detected with the method described above enhance the first peaks found previously with the major SSW distribution and make others appear, especially in November and March. Here, the early warmings in November represent mostly minor SSWs containing likely Canadian Warmings occurring at this period and characterized by an eastward shift of the Aleutian high (Labitzke, [1981](#)).

Beyond mid-December, a continuum of ISSWs is observed during mid-winter, with at least three ISSWs occurring each week. A prominent peak of ISSWs with seven events overlaps the two peaks of major SSWs discussed above in January and February. These two first significant peaks confirm the previously observed trends with major SSWs during mid-winter, that is, some winters have been perturbed by either major or minor warming in mid-January or early February. Furthermore, a third thin peak with seven ISSWs is found at the end of February and March. Finally, some important warmings occur in December and March but with peaks less marked than the three others.

Unsurprisingly, the distribution of FSWs is separated into two major peaks, one before mid-April and the other in early May, pointing out the early and late FSWs, respectively (Butler & Domeisen, [2021](#)). Hence, the median date of all FSWs, which is 15 April, appears to be a good criterion for classifying winters according to their ends. This result is of great interest as it confirms that SSWs and FSWs tend to occur at specific periods and not randomly. Thus, the following section aims to classify all of these winters in order to observe whether major winter evolution scenarios related to these privileged SSW and FSW timings exist.

4. Classification of Winters

This section describes the method employed here to determine the main scenarios of winter evolutions from 1 November to 1 June among the 70 winters since 1950. First, an empirical orthogonal function (EOF) is applied to the zonal mean zonal wind anomaly data set, composed of 70 winters of 213 days, in order to compute the main modes among winters. Here, the zonal wind anomalies are calculated by removing the daily mean over 70 years and dividing afterward by the standard deviation. As the EOF is very sensitive to winters with strong variability, only the first three modes were computed to avoid modes that do not represent observed scenarios (Figure [5](#)). Additionally, in order to confirm that the first three modes are independent from each other, we computed the sampling errors for the eigenvalues associated with the five first EOFs with the following North's "rule of thumb" (North et al., [1982](#)):

$$\delta\lambda_\alpha = \lambda_\alpha(2/N)^{1/2}, \tag{2}$$

where λ_α is the eigenvalue and N is the number of realizations of a particular sample (70 here). The obtained results are displayed in Figure [4](#) and reveal that only the sampling errors associated with the third and fourth eigenvalues overlap by about 20%–30%. Consequently, the first three modes are not a linear mixture of the same eigenvector and can therefore be considered independent. Therefore, these modes illustrate the most important and common features of the winter polar vortex evolution.
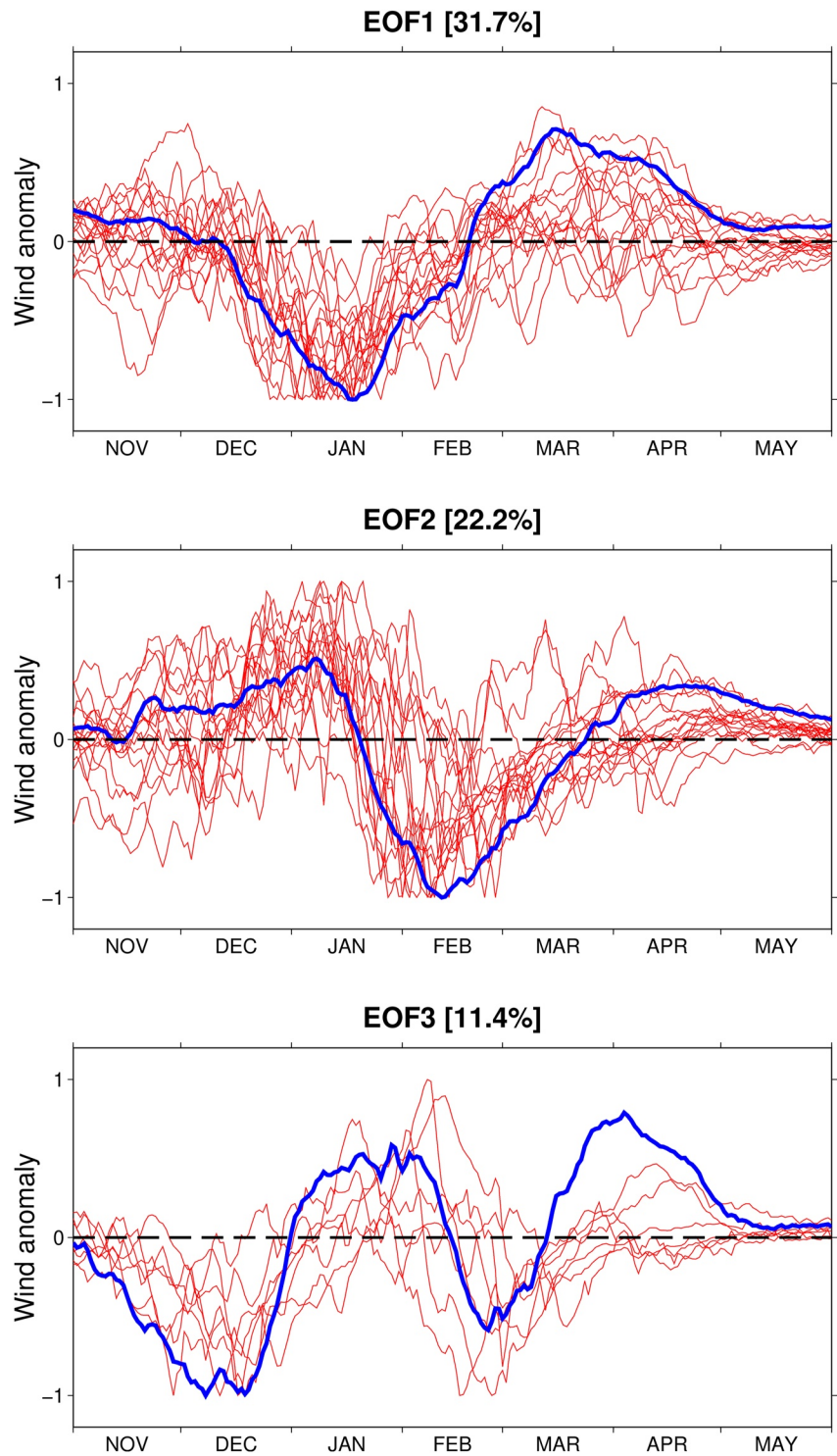
Figure 5. The first three empirical orthogonal functions (EOFs) (blue solid lines) of standardized wind anomalies for the 70 winters between 1950 and 2020 corresponding respectively to (EOF1) 31.7%, (EOF2) 22.2% and (EOF3) 11.4% of the variability. The winters associated with the curve fitting method to EOF1, EOF2, and EOF3 are illustrated by their wind anomaly evolution (red solid lines).

As a result, these EOF patterns illustrate typical physical evolutions of zonal winds in the winter stratosphere where, unsurprisingly, preferential timings of ISSWs contained in winters appear (Figure 5). These first three modes explain 65.3% of the wind fluctuations patterns revealing the main winter typologies and confirming the connection between the mid-winter and the winter end. Indeed, these evolutions reveal how the vortex evolved after an important SSW occurred. Here, EOF1 and EOF2 suggest that there will not be another one before the end of winter when an important SSW occurs in January and February. While, the EOF3 advances that when an important SSW occurs in December, there will be a second one at the end of February. Nonetheless, these suggested evolutions are not faultlessly followed by all associated winters.

The EOF1 (31.7%) represents the scenario with a single ISSW occurring in mid-January (hereafter January mode), and the EOF2 (22.2%) represents the scenario with a single ISSW occurring in February (hereafter February mode). Finally, the EOF3 (11.4%) represents the scenario with two important warmings occurring in December and March (hereafter Double mode). Thus, the patterns of these modes are consistent with the occurrence distribution of important SSW events observed in Figure 3 suggesting that peaks are related to specific scenarios. To perform the classification, we proceeded as follows:

- First, as these scenarios are related to perturbed polar vortex with ISSWs occurring in mid-winter, only the winters for which zonal wind became inferior to $10 \, \text{ms}^{-1}$ once between 15 December and 1 March are selected to avoid considering Canadian warmings and FSWs. As a result, the algorithm identified 50 winters.
- Then, we normalized the three modes as well as the wind anomalies. Afterward, in order to associate these winters to the correct scenarios, a multiple curve fitting is employed by assuming that each winter is a linear combination of the three modes. This technique allows the weighting of the contribution of these three modes via a coefficient. Thus, we can decompose wind anomalies for each winter as follows:

$$\Delta U_{w_i} = k_1 \text{EOF1} + k_2 \text{EOF2} + k_3 \text{EOF3}, \tag{3}$$

where ΔU_{w_i} is the wind anomaly for one winter w_i and k_1, k_2, and k_3 are the coefficients associated to EOF1, EOF2, and EOF3 patterns, respectively.
- Finally, a winter is associated to the scenario with the highest coefficient and whether this coefficient is superior to 0.2 in order to classify only winters with patterns similar to EOF ones.

After several tests, we chose the coefficient threshold of 0.2 that allows for classifying, without making wrong associations, nearly all winters with similar patterns to EOF ones. As a result, 41 winters have been classified, 17 winters in the January mode, 17 winters in the February mode and 7 winters in the Double mode. The nine winters no classified possess similar coefficient magnitudes, all under 0.2, between the three scenarios indicating that they do not follow one precise scenario but more a combination of several different patterns. Consequently, the three main scenarios represent winter evolutions with ISSWs occurring in mid-winter.

After this first classification step, the 20 remaining winters represent the winter scenario nearly no perturbed during the mid-winter. This absence of disturbance makes the method based on the EOF useless to classify them as they do not have enough variability. Consequently, only the end of these winters, that is, when the vortex returns to its summer mode with easterly winds, is studied with a timing criterion. The method to classify FSWs used by Butler and Domeisen (2021) and described in Section 3.1.3 is therefore applied to the remaining winters. However, even though previous studies (Butler & Domeisen, 2021; Waugh & Rong, 2002) generally qualified FSW as "early" or "late" events, we classified the 20 remaining winters, similarly to Hauchecorne et al. (2022), into either radiative final warming mode (hereafter RFW mode) or dynamical final warming mode (hereafter DFW mode) for illustrating both their timing and the physical processes triggering them. Even though the DFW and RFW modes are under modes of the same scenario, they will be treated separately for the remaining of this study. As a result, the algorithm classified five and 15 winters in the RFW and DFW modes at the end of this last step, respectively. The result of this last classification is shown in Figure 7. The distribution of the 61 associated winters among these four scenarios and their occurrence over time are shown in Appendix A.

Figure 6. Evolutions of the zonal mean zonal wind at 10 hPa and 60°N for each winter (thin red lines) classified into the first three modes identified: the January single warming mode (a), the February single warming mode (b) and the Double warming mode (c). The blue solid and dashed lines show the mean and the standard deviation, respectively.

5. Characterization of Different Scenarios

Figure 6 illustrates the three scenarios identified with the principal component analysis by showing the mean evolutions of the wind at 10 hPa and 60°N of the associated winters. EOF evolutions (Figure 5) show clear
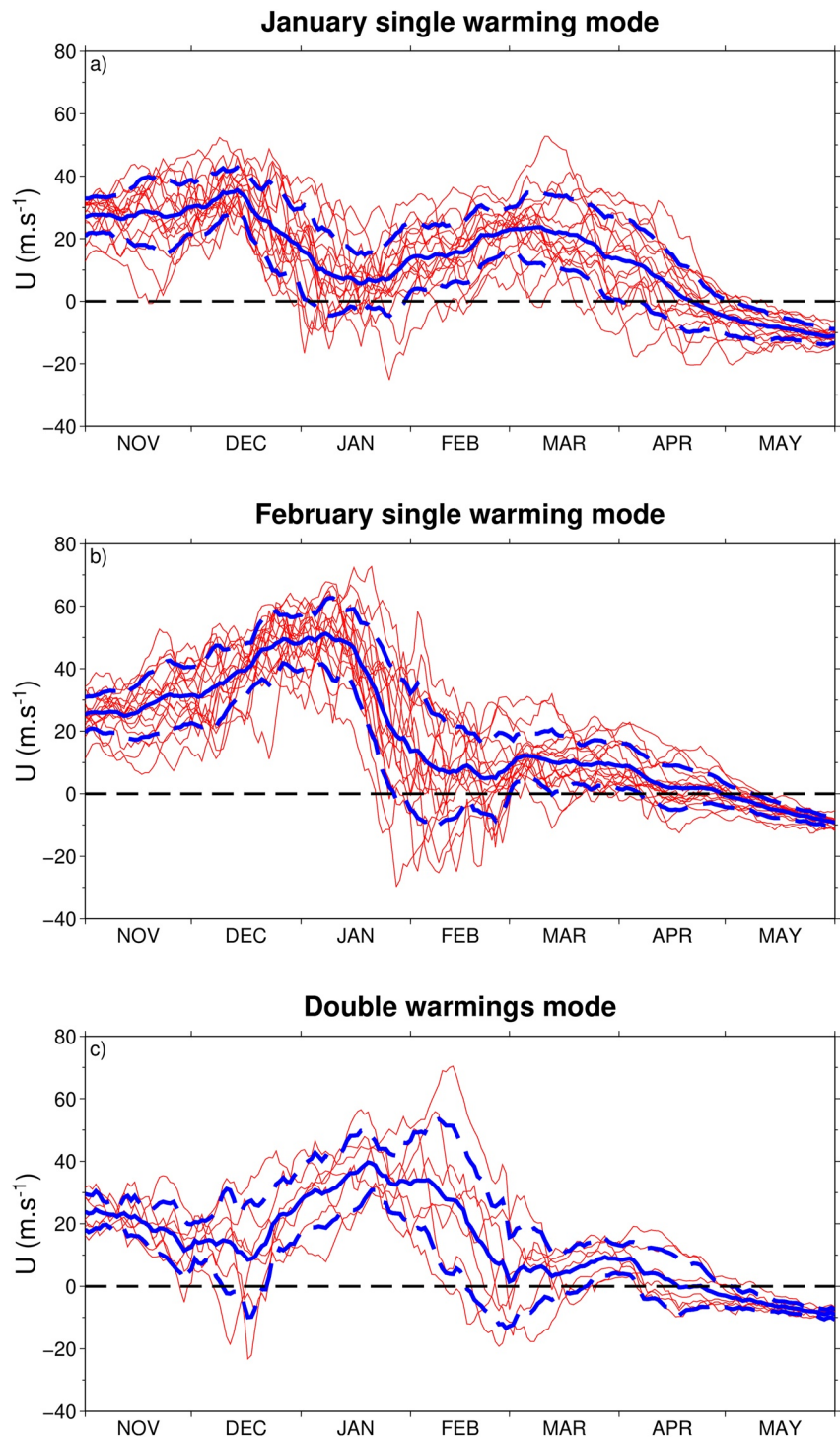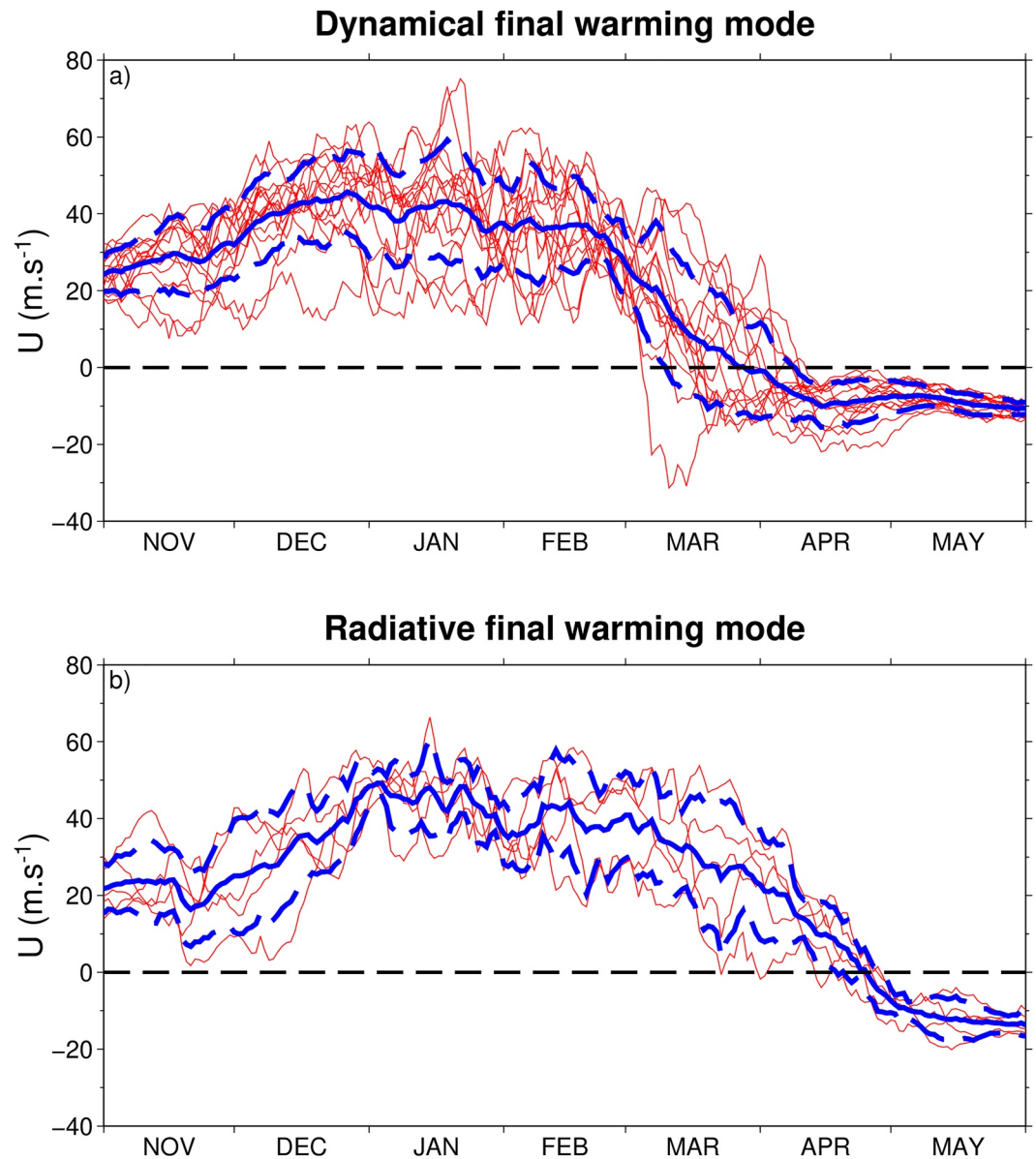
Figure 7. Evolutions of the zonal mean zonal wind at 10 hPa and 60°N for remaining winters (thin red lines) classified into the last scenario with two under-modes: the Dynamical final warming mode (a) and the Radiative final warming mode (b). The blue solid and dashed lines show the mean and the standard deviation, respectively.

anti-correlations between mid-winter and winter end. For instance, clear anti-correlation is found between January and March and between February and April for the EOF1 and EOF2, respectively, while the EOF3 presents an anti-correlation with a shorter interval between the end of February and early April. The anti-correlations between the early winter and the mid-winter are less marked in these modes. Nonetheless, this result confirms the conclusion by Hauchecorne et al. (2022), that is, the polar vortex on a given month is anti-correlated with its state 2–3 months earlier. Hence, according to the mean evolutions of these modes, the instant when important SSW occurs is a critical indicator for understanding the winter evolution afterward. The last winter scenario with its two under-mode, dynamical or radiative final warming, is also illustrated by the mean stratospheric wind evolutions at 10 hPa and 60°N of the associated winters in Figure 7. Table 1 reports the number of major SSWs, Canadian warmings, and FSW types among winters composing the four scenarios, determined with the methods detailed previously in Section 3.1, as well as the mean date of FSWs and their standard deviation.

Table 1
Number of Radiative, Dynamical and Unclassified Final Stratospheric Warmings (FSWs) Among the Winters Classified Into the Four Scenarios

FSW type	January mode	February mode	Double mode	DFW mode	RFW mode
Radiative	10	14	3	0	5
Dynamical	5	3	3	15	0
Unclassified	2	0	1	0	0
Mean date of FSWs	21 April	28 April	20 April	28 March	26 April
Standard deviation	13 days	12 days	13 days	11 days	4 days
Major SSWs	15	13	4 and 6	1	1
Early warmings	1	1	1	2	2

Note. The mean date of FSWs is displayed with the standard deviation. The number of winter with at least one major SSW and with an early warming are given as well.

For the January mode (Figure 6a), the vortex is, on average, enhanced during November even though Canadian warmings can occur at this period but without preventing the occurring of ISSWs in January. Indeed, the common point of these winters is that the vortex is slowed from mid-December due to the important SSW, very often major (almost 90% here), occurring around mid-January. Afterward, the vortex forms again with winds exceeding 20 ms^{-1} on average from mid-February. Finally, the vortex falls down from the end of March to enter its summer mode preferentially with a radiative end or, sometimes, a dynamical end (see Table 1). The supposed reason these winter evolutions do not have a very marked preference end is that their SSW occur early enough in winter, making time necessary for the reforming of the vortex. According to Table 1, 10 winters finish with a radiative end, five finish with a dynamical end, and two winters remain unclassified. The FSWs occur on average on 21 April with a standard deviation of 13 days, confirming that ISSWs occurring in January do not influence the end type.

For the February mode (Figure 6b), the vortex is on average very strongly reinforced at the beginning of winter with winds lying from more than 20 ms^{-1} at the start of November to more than 40 ms^{-1} at the start of January. Then, the vortex is strongly decelerated from mid-January due to the important SSW occurring in February. Following this important SSW, which is often a major SSW, the vortex does not benefit from the necessary scale time to recover its previous state. Additionally, due to the seasonal variation in the radiation, the vortex strength starts to decrease gradually, preventing it from reaching its mid-winter strength. Therefore, the vortex remains very weak during the March month with winds at about 10 ms^{-1} on average. For finishing, the vortex falls entirely at the end of April with a late and radiative end. These results are confirmed by Table 1 reporting that for more than 80% of winters composing the February mode, the algorithm has identified a radiative end occurring on average on 28 April with a standard deviation of 12 days. Furthermore, among these 17 winters, 13 major SSW events occurred, confirming that the vigorous intensity of the vortex breaking in February is strongly correlated to a radiative end. However, the warming in February did not prevent a dynamic end for three winters suggesting that other mechanisms drive the end type in addition of the timing of important SSW in mid-winter.

These results are in agreement with those found in Hu et al. (2014) who reported that winters with SSWs have a higher probability to finish with a late FSW than winters without SSWs.

For the Double warmings mode (Figure 6c), a first important SSW, major for more than half of winters, occurs around mid-December, causing the weakening of the vortex as soon as the November month has started. After this first significant warming, the vortex is reinforced until mid-January with winds exceeding 30 ms^{-1} on average. Then a second important SSW, nearly every-time major, occurs at the end of February, weakening the vortex again. This last warming occurring lately in the winter prevents a complete restoration of the vortex and, therefore, leads it to its end. Thus, the mean final transition pattern of the Double mode is very similar to the one of the February mode. In contrast, there are as many winters with a radiative end as a dynamic end. The date of FSWs is, on average, on 20 April and a standard deviation of 13 days. This result confirms that the winter end, partly influenced by ISSWs' timings, is dynamically and radiatively driven (Butler & Domeisen, 2021; Salby & Callaghan, 2007). Winters with early FSWs possess a similar mechanism to mid-winter SSWs, that is, predominantly wave-driven, while late FSWs occur when winds weaken due to the changing solar radiation requiring less wave activity to break the vortex definitely (Vargin et al., 2020). However, these observed trends for the Double mode suffer from a few numbers of associated winters limiting their robustness. Therefore, more winters are necessary to confirm whether there is a preferred end type associated with this scenario.

While for the Dynamical and the Radiative modes belonging to the unperturbed vortex scenario, their mean winter evolutions are similar, that is, with no ISSWs from 15 December to 1 March, but with different end types (Figures 7a and 7b). The starting of winters is characterized by a strong enhancement of the polar vortex, with sometimes the presence of Canadian warmings occurring in November or in early December. Then, as the mid-winter is not perturbed by major SSWs, the polar vortex remains stable and strong until the arrival of the spring and the FSW. Regarding the Dynamical-mode, the FSW date is on average on 28 March with a standard deviation of 11 days, while for the Radiative-mode, the FSW date is on average on 26 April with a standard
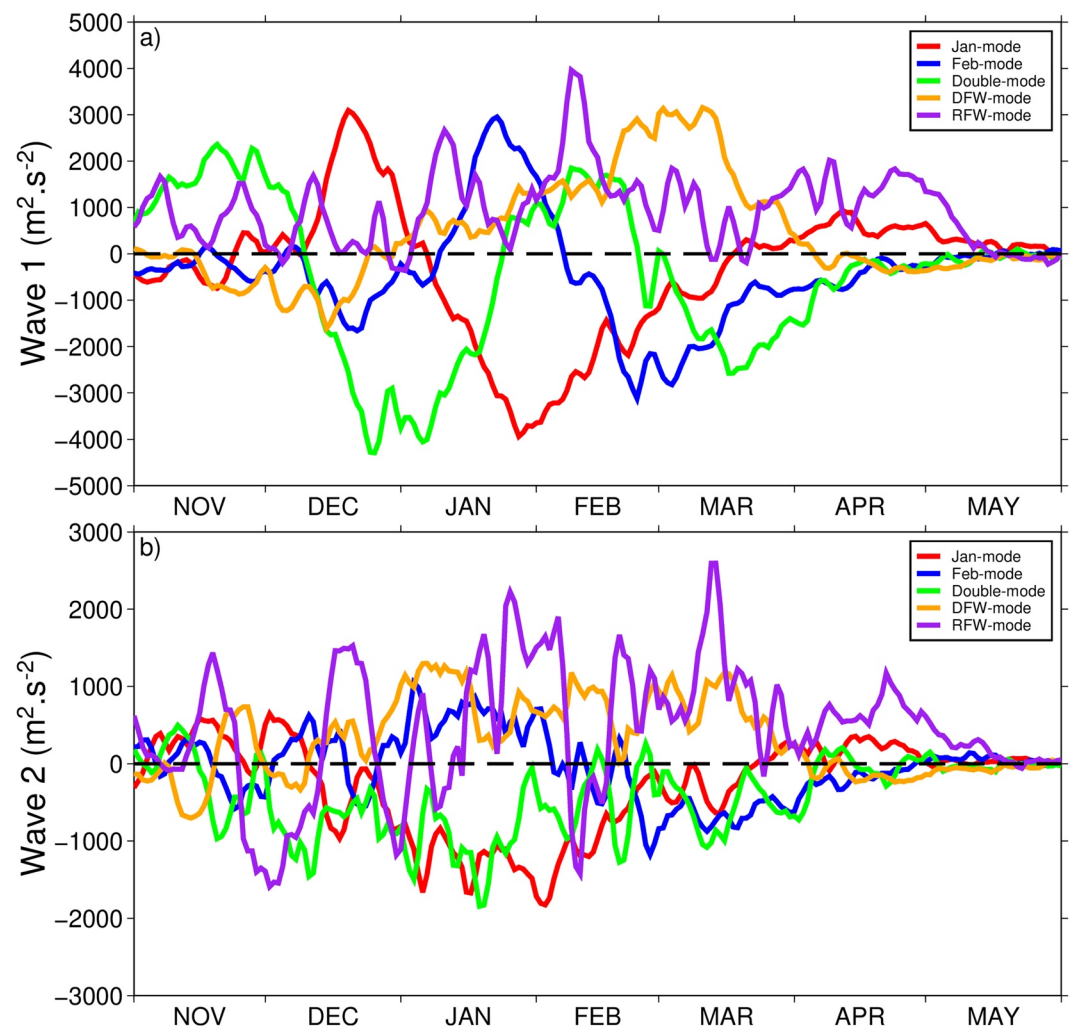
Figure 8. Mean evolutions of waves 1 (a) and 2 (b) amplitude anomalies for each scenario during the extended winter.

deviation of 4 days. Thus, there is almost 1 month on average separating the final warming dates between winters with a dynamical end and a radiative end. Finally, the unequal distribution of winters without ISSWs according to their FSW's timing, early and dynamical (15 winters) or late and radiative (five winters), is consistent with the trend observed in Hu et al. (2014).

How the timing of the ISSWs and FSWs for each scenario is preconditioned by the evolutions of the activities of planetary waves 1 and 2 is studied in the next section.

6. Evolution of Wave-1 and Wave-2 Activities

Figure 8 shows the mean anomalies evolutions of the planetary waves 1 and 2 during winter for each scenario obtained after to have removed the daily climatology computed over the 70 years. For all scenarios apart from the Double mode, the wave-1 anomalies remain near zero until early December, pointing out that the other modes follow the seasonal wave-1 activity increasing. In contrast, a constant strong positive wave-1 anomaly characterizes the exception of the Double mode in the same period preceding the important SSW occurring in December. Beyond early December, the wave-1 activities associated with the modes separate each other. The wave-2 anomalies for each scenario oscillate overall around zero until early December but with smaller amplitudes than for wave-1.

For the January mode, the mean anomaly amplitude of wave-1 strongly increases from early to mid-December, reaching its highest amplitude of more than 3,000 m^2 s^{-2}, and then drops abruptly to reach an amplitude of almost −4,000 m^2 s^{-2} at the end of January. Afterward, the wave-1 anomaly increases again to become positive in mid-April and then starts to decrease definitely until the end of winter. On the other hand, the wave-2 anomaly remains overall negative, with a peak of almost −2,000 m^2 s^{-2} in early February. Therefore, winters associated with the January mode are mostly wave-1 driven. The evolution of the wave-1 anomaly amplitude is in perfect consistency with the formation and the reinforcement of the vortex in early winter as well as during February and the occurrence of the major SSW and FSW around mid-January and mid-April, respectively indeed, because upward propagating planetary waves from the troposphere to the stratosphere are possible only in a westerly circulation.

Regarding the February mode, the wave-1 anomaly drops from early December to mid-December, where a first minimum is reached, about −1,500 m^2 s^{-2}. Afterward, the wave-1 activity strongly increases to reach a peak after mid-January with a similar amplitude, almost 3,000 m^2 s^{-2} that the one found in mid-December for the January mode. Then, the wave-1 anomaly drops suddenly to become negative and reaches the second minimum of −3,000 m^2 s^{-2} at the end of February. Beyond this moment, the wave-1 activity remains weaker than the seasonal climatology until the end of the winter. A similar evolution is found for the wave-2 anomaly, first increasing after December to reach a maximum with a positive peak of around 1,000 m^2 s^{-2} at mid-January, and then dropping to reach a minimum at the end of February before remaining negative until the winter end. Thus, this result shows that wave-1 and wave-2 drive the stratospheric circulation for winters associated with the February mode. As for the January mode, these evolutions are perfectly consistent with the vortex formation and its reinforcement during November and December and with the major SSW and the radiative end occurring in February and the end of April, respectively.

For the Double mode, after the positive anomaly in November, the wave-1 activity starts to decrease from early December until the end of December to reach a negative minimum of less than −4,000 m^2 s^{-2} while the wave-2 anomaly decreases constantly. Then, the wave-1 anomaly increases until early February to reach an activity similar to the November one, around 1,500 m^2 s^{-2}. Afterward, the wave-1 anomaly drops again when the second important SSW occurs and reaches a second negative minimum in mid-March, almost −3,000 m^2 s^{-2}. Finally, the wave-1 anomaly remains negative until the winter end. A similar evolution of the wave-2 activity to the January mode is found for the Double mode, that is, the wave-2 anomaly remains overall negative during winter. Thus, these mean evolutions of wave-1 anomalies are coherent with the timing of the two ISSWs occurring in the winters associated with the Double mode. Therefore, the first and the second ISSWs of these winters, occurring in mid-December and at the end of February, respectively, are preconditioned mostly by a wave-1 activity.

Consistently with the zonal wind evolutions shown in Figure 7, similar trends in the wave activities are found between the DFW and RFW modes. Indeed, the wave-1 and wave-2 activities associated with both modes remain overall stronger than the seasonal activity. The RFW mode is characterized by a wave-1 anomaly increasing slightly from early January to mid-February to reach a maximum of almost 4,000 m^2 s^{-2} and then dropping progressively until the end of May. While, for the DFW mode, the wave-1 anomaly increases from mid-December to reach a maximum in mid-March of 3,000 m^2 s^{-2} and then drops suddenly to reach an anomaly near zero in early April. We notice that, as expected, the DFW mode possesses a wave-1 activity stronger than the RFW mode from mid-February to mid-March. However, the opposite is found for the wave-2 activity in the same period. Regarding the wave-2 anomalies, the DFW mode possesses a general constant positive anomaly around 1,000 m^2 s^{-2} from early January to mid-March, while an oscillating evolution is observed for the RFW mode. A strong drop in the wave-2 activity is observed in early February for the RFW mode reaching less than −1,000 m^2 s^{-2}, coinciding that the maximum of nearly 4,000 m^2 s^{-2} reached by the wave-1 anomaly. After this drop, the wave-2 activity increases to reach and finish with the same amplitude as the DFW mode. Even though a notable peak not expected in March of about 2,500 m^2 s^{-2} for the RFW mode is found, before decreasing until the end of May.

7. Discussion

Thus, the new classification technique employed here divided the 70 winters among four scenarios identified, representing each typical evolution of the stratospheric circulation during winter. However, as this method used to build the four composites is based on the stratospheric zonal wind patterns from 1 November to 1 June, the
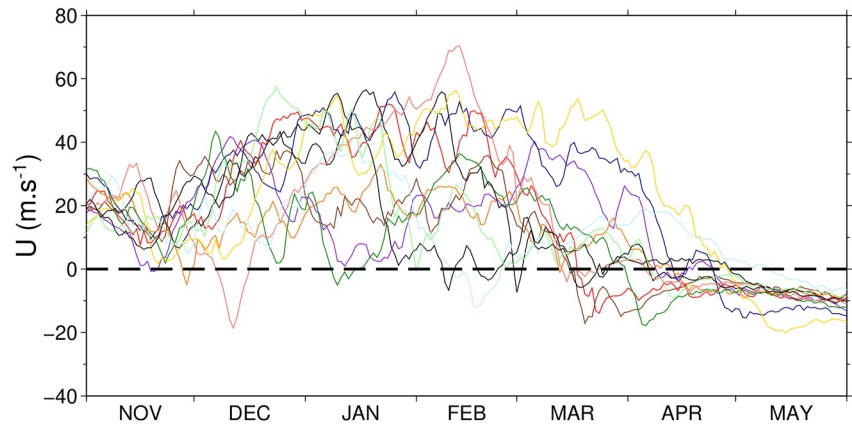
Figure 9. Evolution of the zonal mean zonal wind at 10 hPa and 60°N for each winter with an important warming occurring in November.

algorithm might have proceeded to the wrong winter associations. For instance, winters with an important SSW occurring at the end of January can be associated with the January mode while they should be associated with the February mode or inversely (see Figures 6a and 6b).

Nevertheless, the mean stratospheric zonal wind patterns found for each scenario testify that the algorithm correctly classified most of the winters. Additionally, their consistency with the mean evolutions of the waves' amplitudes constitutes further evidence that the algorithm identified real distinct scenarios with specific dynamical behaviors. Indeed, for example, only the quasi-stationary wave-1 tends to dominate during the pre-warming phase for winters associated with the January mode. While for the winters associated with the February mode, waves 1 and 2 tend to play an average role in the occurrence of the important SSW.

The mean evolutions of wave-1 anomaly amplitudes, especially from December, follow different typologies more marked with greater magnitude than the mean evolutions of wave-2 anomaly amplitudes. The main reason is that wave-1, in statistics, tends to play a significant role each time the vortex is strongly perturbed regardless of the vortex geometry, that is, either displacement or splitting events (Bancalá et al., 2012; Barriopedro & Calvo, 2014). Another reason is that the wave-2 anomaly evolutions for each winter are more abrupt and sudden than the constant evolutions observed for wave-1 prior to the important SSW occurring (not shown here). Consequently, the mean evolutions of wave-2 anomaly amplitudes shown in this study are less suitable markers than wave-1 activities to illustrate the different dynamics between scenarios. Finally, the common evolutions of the wave-1 amplitudes during November month are mainly due to the seasonal cycle of the wave activity. Beyond early December, the reasons the modes separate from each other remain unknown. Investigating the mechanisms influencing the winter unfolding and causing the divergence from this climatology of the wave activity for each mode should be pursued in future studies. The observed precursors in the mesosphere in Angot et al. (2012) should be considered a first lead up to 2 months before minor and major SSWs occur in the stratosphere.

Interestingly, from mid-February to mid-March, the wave-1 and wave-2 wave activities of the DFW mode are stronger and weaker than those of the RFW mode. However, as the DFW mode is expected to have stronger wave activity than the RFW mode at this period (Vargin et al., 2020), this result suggests, first, that dynamical FSWs are triggered mainly by the wave-1 activity and, second, that the wave-1 activity plays a role, more or less significant systematically, in all FSWs' triggering.

Identifying important warmings occurring in early winter, sometimes classified in the literature as Canadian warmings, which rarely reverse the zonal winds, is undertaken to investigate their influence on winter unfolding. Here, early warming is detected when the zonal wind became once inferior to 10 ms^{-1} during November. Thanks to this wind criterion, 12 warming events have been detected, including the events classified as Canadian warmings by Labitzke (1981). According to the result of the classification, the winters with early warming do not have a preferred scenario (see Table 1), confirming the ability of the algorithm to capture the general trend even when unusual events occur. This result is confirmed in Figure 9 showing how the 12 winter evolutions with early warming identified in November follow different patterns.

The causes why this early warming does not prevent or influence the occurrence and the timing of an important SSW in the following months are not investigated here. Nevertheless, the likely reasons for this behavior are that early warmings are often weak, and the polar vortex is rapidly reinforced due to the radiation cooling. Furthermore, the Canadian warmings among these events mainly impact the lower stratosphere (Manney et al., 2001).

When we compare with the classifications carried out by Charlton and Polvani (2007), Mitchell et al. (2013), Barriopedro and Calvo (2014) and Afargan-Gerstman and Domeisen (2020) (not shown here), only the February mode tends to be associated with split events. Otherwise, the different scenarios identified here are neither related to a specific vortex geometry type, a certain wave geometry, or a precise downward impact after major SSWs. This result was expected as the vortex geometry is unrelated to a distinct wave geometry. Indeed, Bancalá et al. (2012), who investigated the wave geometry in the prewarming phase, classified major SSWs according to the dominant zonal wavenumber (wave-1 or wave-2 events). Additionally, Barriopedro and Calvo (2014) examined the El Nino-Southern Oscillation (ENSO) phase, either El Nino (EL) or La Nina (LN), during major SSWs and found amplification of wavenumber 1 preceding SSWs during EL phase and amplification of wavenumber 2 preceding SSWs during LN phase. However, the evolution of the vortex geometry toward a splitting or a displacement event during SSWs does not have a privileged ENSO phase or a specific wave geometry. Moreover, the vortex splitting event arises not only with a strong wave-2 activity but also with significant wave-1 activity.

Consequently, the timing of ISSWs and FSWs and, therefore, the winter typologies are independent of these characteristics. This absence of correlation is not surprising as the classification carried out here is based on the stratospheric circulation patterns influenced by the timing of ISSWs and FSWs, while the vortex structure, as well as the dominant wavenumber during the pre-warming phase, are influenced by the ENSO phase (Barriopedro & Calvo, 2014). Indeed, this new way to classify SSWs and FSWs, that is, focusing on winter typologies rather than only on the most extreme events, reveals how the mid-winter is connected to the winter end. Thus, the three perturbed scenarios identified here confirm the result found in Hauchecorne et al. (2022), especially from the mid-winter, that is, the vortex state on a given month is anti-correlated with its state 2–3 months earlier and are therefore further evidence of the stratospheric memory existence.

8. Conclusions

In this study, we have classified 61 winters among the 70 NH winters from 1950 to 2020 into four distinct scenarios with a new technique based on EOF analysis of the evolution of the anomaly of stratospheric zonal mean zonal winds extracted from the ERA5 package at the edge of the polar vortex. These four scenarios are influenced by the timings of ISSWs, including major and minor SSWs, and FSWs, giving an overview of the stratospheric memory, that is, how the mid-winter is connected to the winter end. The first advantage of this new method of classification is to focus on the winter typologies and not only on the major SSW events extending the number of winters classifiable.

Thus, the algorithm identified three perturbed scenarios with ISSWs occurring in mid-winter: the January mode (17 winters), the February mode (17 winters), and the Double mode (seven winters). Here nine winters among the perturbed winters possess atypical patterns and remain unclassified. Most of the time, the January mode is characterized by a major SSW occurring in mid-January and afterward a reinforcement of the vortex to finish preferentially radiatively or sometimes with a dynamical FSW. Here, we found that among the winters with an important SSW in January, 30% have a dynamical FSW, and 60% have a radiative FSW. Strong reinforcement of the vortex characterizes the February mode in early winter, often followed by a major SSW occurring in February, generally finishing (for 82% of cases here) with a radiative FSW confirming that ISSWs' timings influence the winter end. Winters with ISSWs tend to finish with a radiative FSW. Finally, the Double mode is characterized by a first important SSW occurring in mid-December and a second important SSW at the end of February to finish either with a radiative or dynamical end. However, contrary to the January and February modes, the few winters associated with the Double mode make it difficult to infer a robust trend for the privileged FSW type. Therefore, according to our results, the ISSWs' timings influence but are not the only mechanisms responsible for the triggering timing of FSWs.

Accordingly, the conclusion in Hauchecorne et al. (2022) is confirmed here with these first three scenarios, that is, the vortex on a given month is anti-correlated with its state 2–3 months earlier.

The last scenario represents undisturbed winters classified into two under-modes according to their end types, either late and radiative (five winters) or early and dynamical (15 winters), confirming that winters without ISSWs tend to finish with an early FSW.

Additionally, the mean evolutions of wave amplitudes associated with each scenario, especially the wave-1 evolutions, are consistent with the zonal wind patterns found, confirming the different dynamics behaviors between each scenario in the pre-warming phase. After a comparison with the classifications done by Mitchell et al. (2013), Barriopedro and Calvo (2014) and Afargan-Gerstman and Domeisen (2020), only the February mode tends to be related to a splitting vortex type after that important SSW occurred. Otherwise, the scenarios found here are not related to a typical vortex geometry, wave geometry, or tropospheric response. Furthermore, the unfolding of winters is not affected by ISSWs occurring in early winter, which are Canadian warmings for most of them, mainly because they are often weak and the polar vortex is rapidly reinforced by the radiative cooling and also as they tend to impact only the lower stratosphere (Manney et al., 2001).

Consequently, the main interests of this new classification are that the EOF analysis confirms mathematically that the observed winter patterns with similar preferential SSWs' timings follow independent modes illustrating typical physical evolutions. Second, this new way to classify ISSWs and FSWs according to their timings and impacts on the winter evolution aims to establish the connection between the mid-winter and the winter end. Finally, the objective classification of winters into these modes of variability improves our understanding of the stratosphere state, which is essential for seasonal forecasting in the lower layers. However, further researches are necessary to explain why the wintertime stratospheric winds follow these typologies and why one scenario occurs rather than another. Thus, several significant questions remain suspended:

- What are the precursors responsible for each scenario and the SSW timings?
- What causes the different wave-1 and wave-2 activities between the scenarios?
- On what depends on the winter end type when the polar vortex remains very strong?

and should be investigated in the future, thanks to the four composites determined here. Here, the wave-1 activities associated with the scenarios separate each other from early December, suggesting that the mechanisms responsible for their occurrence act in the previous months. A first lead should be the observed temperature anomalies in the mesosphere in Angot et al. (2012) up to 2 months before minor and major SSWs occur. Finally, further research on these winter scenarios can contribute to better modeling the stratospheric wintertime wind evolutions in climate models, improving their overall weather forecasting (Figure A1).

Appendix A: Distribution of the 70 Winters

1. January single warming mode: (1950/1951, 1952/1953, 1954/1955, 1959/1960, 1967/1968, 1969/1970, 1970/1971, 1976/1977, 1984/1985, 1997/1998, 2001/2002, 2002/2003, 2003/2004, 2005/2006, 2011/2012, 2012/2013, 2018/2019).
2. February single warming mode: (1956/1957, 1957/1958, 1962/1963, 1972/1973, 1978/1979, 1980/1981, 1982/1983, 1986/1987, 1988/1989, 1989/1990, 1990/1991, 1994/1995, 2007/2008, 2008/2009, 2009/2010, 2016/2017, 2017/2018).
3. Double warmings mode: (1951/1952, 1965/1966, 1968/1969, 1979/1980, 1987/1988, 1998/1999, 2000/2001).
4. Unperturbed mode:
   Dynamical final warming mode: (1955/1956, 1958/1959, 1960/1961, 1963/1964, 1973/1974, 1974/1975, 1975/1976, 1985/1986, 1992/1993, 1995/1996, 1999/2000, 2010/2011, 2013/2014, 2014/2015, 2015/2016).
   Radiative final warming mode: (1961/1962, 1964/1965, 1966/1967, 1996/1997, 2019/2020).
5. Unclassified winters: (1953/1954, 1971/1972, 1977/1978, 1981/1982, 1983/1984, 1991/1992, 1993/1994, 2004/2005, 2006/2007).
6. Winters with an early warming: (1952/1953, 1958/1959, 1966/1967, 1968/1969, 1974/1975, 1976/1977, 1979/1980, 1987/1988, 1996/1997, 2000/2001, 2009/2010, 2016/2017).
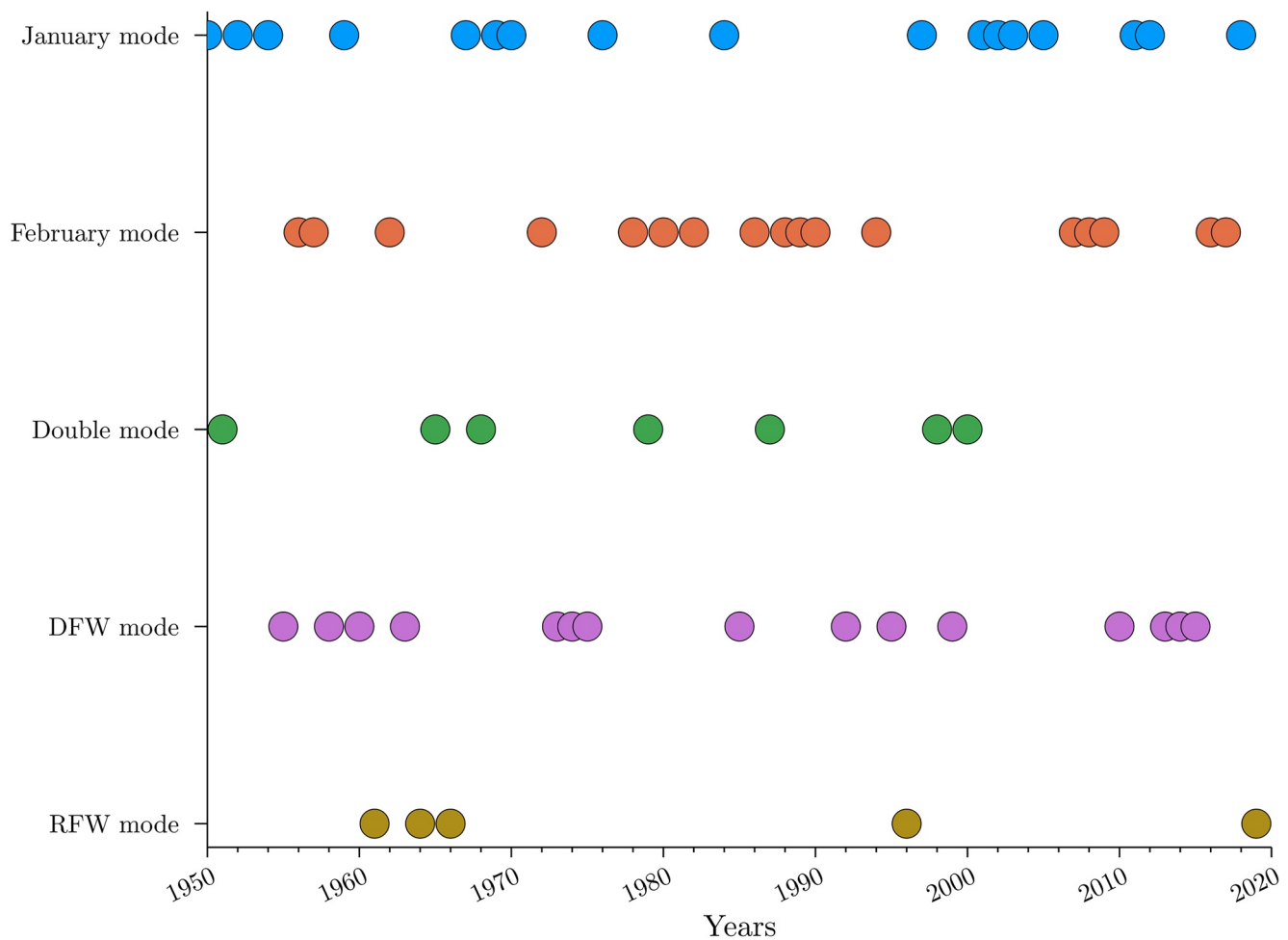
Figure A1. Distribution of the 70 winters among the five scenarios over time.

Data Availability Statement

How to access ERA5 data on pressure levels from 1950 to the present is explained on the ECMWF website: https://confluence.ecmwf.int/display/CKB/How+to+download+ERA5#HowtodownloadERA5-OptionB:Download-loadERA5familydatathatisNOTlistedintheCDSonlinecatalogue-SLOWACCESS Hersbach et al. (2018) was downloaded from the Copernicus Climate Change Service (C3S) Climate Data Store. Bell et al. (2020) was downloaded from the Copernicus Climate Change Service (C3S) Climate Data Store. The results contain modified Copernicus Climate Change Service information 2020. Neither the European Commission nor ECMWF is responsible for any use that may be made of the Copernicus information or data it contains.

References

Afargan-Gerstman, H., & Domeisen, D. (2020). Pacific modulation of the North Atlantic storm track response to sudden stratospheric warming events. *Geophysical Research Letters*, *47*(2), e2019GL085007. https://doi.org/10.1029/2019GL085007

Andrews, D., Holton, J., & Leovy, C. (1987). *Middle atmosphere dynamics*. Elsevier Science.

Angot, G., Keckhut, P., Hauchecorne, A., & Claud, C. (2012). Contribution of stratospheric warmings to temperature trends in the middle atmosphere from the lidar series obtained at haute-provence observatory (44°N). *Journal of Geophysical Research*, *117*(D21), D21102. https://doi.org/10.1029/2012JD017631

Baldwin, M., & Dunkerton, T. (2001). Stratospheric harbingers of anomalous weather regimes. *Science*, *294*(5542), 581–584. https://doi.org/10.1126/science.1063315

Baldwin, M. P., Ayarzagüena, B., Birner, T., Butchart, N., Butler, A. H., Charlton-Perez, A. J., et al. (2021). Sudden stratospheric warmings. *Reviews of Geophysics*, *59*(1), e2020RG000708. https://doi.org/10.1029/2020RG000708

Bancalá, S., Krüger, K., & Giorgetta, M. (2012). The preconditioning of major sudden stratospheric warmings. *Journal of Geophysical Research*, *117*(D4), D04101. https://doi.org/10.1029/2011JD016769

Barriopedro, D., & Calvo, N. (2014). On the relationship between ENSO, stratospheric sudden warmings, and blocking. *Journal of Climate*, *27*(12), 4704–4720. https://doi.org/10.1175/JCLI-D-13-00770.1

Bell, B., Hersbach, H., Berrisford, P., Dahlgren, P., Horányi, A., Muñoz Sabater, J., et al. (2020). ERA5 hourly data on pressure levels from 1950 to 1978 (preliminary version). [dataset]. Copernicus Climate Change Service (C3S) Climate Data Store (CDS). Retrieved from https://cds.climate.copernicus-climate.eu/cdsapp#!/dataset/reanalysis-era5-pressure-levels-preliminary-back-extension?tab=overview

Butler, A. H., & Domeisen, D. I. V. (2021). The wave geometry of final stratospheric warming events. *Weather and Climate Dynamics*, *2*, 453–474. https://doi.org/10.5194/wcd-2-453-2021

Butler, A. H., Seidel, D. J., Hardiman, S. C., Butchart, N., Birner, T., & Match, A. (2015). Defining sudden stratospheric warmings. *Bulletin of the American Meteorological Society*, *96*(11), 1913–1928. https://doi.org/10.1175/BAMS-D-13-00173.1

Butler, A. H., Sjoberg, J. P., Seidel, D. J., & Rosenlof, K. H. (2017). A sudden stratospheric warming compendium. *Earth System Science Data*, *9*(1), 63–76. https://doi.org/10.5194/essd-9-63-2017

Charlton, A. J., O'Neill, A., Lahoz, W. A., & Berrisford, P. (2005). The splitting of the stratospheric polar vortex in the southern hemisphere, September 2002: Dynamical evolution. *Journal of the Atmospheric Sciences*, *62*(3), 590–602. https://doi.org/10.1175/JAS-3318.1

Charlton, A. J., & Polvani, L. M. (2007). A new look at stratospheric sudden warmings. Part I: Climatology and modeling benchmarks. *Journal of Climate*, *20*(3), 449–469. https://doi.org/10.1175/JCLI3996.1

Charlton-Perez, A. J., Ferranti, L., & Lee, R. W. (2018). The influence of the stratospheric state on North Atlantic weather regimes. *Quarterly Journal of the Royal Meteorological Society*, *144*(713), 1140–1151. https://doi.org/10.1002/qj.3280

Dee, D. P., Uppala, S. M., Simmons, A. J., Berrisford, P., Poli, P., Kobayashi, S., et al. (2011). The ERA-interim reanalysis: Configuration and performance of the data assimilation system. *Quarterly Journal of the Royal Meteorological Society*, *137*(656), 553–597. https://doi.org/10.1002/qj.828

Domeisen, D. I. (2019). Estimating the frequency of sudden stratospheric warming events from surface observations of the North Atlantic oscillation. *Journal of Geophysical Research: Atmospheres*, *124*(6), 3180–3194. https://doi.org/10.1029/2018JD030077

Fusco, A. C., & Salby, M. L. (1999). Interannual variations of total ozone and their relationship to variations of planetary wave activity. *Journal of Climate*, *12*(6), 1619–1629. https://doi.org/10.1175/1520-0442(1999)012<1619:IVOTOA>2.0.CO;2

Hauchecorne, A., Claud, C., Keckhut, P., & Mariaccia, A. (2022). Stratospheric final warmings fall into two categories with different evolution over the course of the year. *Communications Earth & Environment*, *3*(1), 4. https://doi.org/10.1038/s43247-021-00335-z

Hersbach, H., Bell, B., Berrisford, P., Biavati, G., Horányi, A., Muñoz Sabater, J., et al. (2018). ERA5 hourly data on single levels from 1979 to present. [dataset]. Copernicus Climate Change Service (C3S) Climate Data Store (CDS). Retrieved from https://cds.climate.copernicus-climate.eu/cdsapp#!/dataset/reanalysis-era5-pressure-levels-preliminary-back-extension?tab=overview

Hersbach, H., Bell, B., Berrisford, P., Hirahara, S., Horányi, A., Muñoz-Sabater, J., et al. (2020). The ERA5 global reanalysis. *Quarterly Journal of the Royal Meteorological Society*, *146*(730), 1999–2049. https://doi.org/10.1002/qj.3803

Hu, J., Ren, R., & Xu, H. (2014). Occurrence of winter stratospheric sudden warming events and the seasonal timing of spring stratospheric final warming. *Journal of the Atmospheric Sciences*, *71*(7), 2319–2334. https://doi.org/10.1175/JAS-D-13-0349.1

Kodera, K., Mukougawa, H., Maury, P., Ueda, M., & Claud, C. (2016). Absorbing and reflecting sudden stratospheric warming events and their relationship with tropospheric circulation. *Journal of Geophysical Research: Atmospheres*, *121*(1), 80–94. https://doi.org/10.1002/2015JD023359

Krüger, K., Naujokat, B., & Labitzke, K. (2005). The unusual midwinter warming in the Southern Hemisphere stratosphere 2002: A comparison to Northern Hemisphere phenomena. *Journal of the Atmospheric Sciences*, *62*(3), 603–613. https://doi.org/10.1175/JAS-3316.1

Labitzke, K. (1981). Stratospheric-mesospheric midwinter disturbances—A summary of observed characteristics. *Journal of Geophysical Research*, *86*(C10), 9665–9678. https://doi.org/10.1029/JC086iC10p09665

Limpasuvan, V., Thompson, D. W. J., & Hartmann, D. L. (2004). The life cycle of the Northern Hemisphere sudden stratospheric warmings. *Journal of Climate*, *17*(13), 2584–2596. https://doi.org/10.1175/1520-0442(2004)017<2584:TLCOTN>2.0.CO;2

Manney, G. L., Sabutis, J. L., & Swinbank, R. (2001). A unique stratospheric warming event in November 2000. *Geophysical Research Letters*, *28*(13), 2629–2632. https://doi.org/10.1029/2001GL012973

Mariaccia, A., Keckhut, P., Hauchecorne, A., Claud, C., Le Pichon, A., Meftah, M., & Khaykin, S. (2022). Assessment of ERA-5 temperature variability in the middle atmosphere using Rayleigh lidar measurements between 2005 and 2020. *Atmosphere*, *13*(2), 242. https://doi.org/10.3390/atmos13020242

Marlton, G., Charlton-Perez, A., Harrison, G., Polichtchouk, I., Hauchecorne, A., Keckhut, P., et al. (2021). Using a network of temperature lidars to identify temperature biases in the upper stratosphere in ECMWF reanalyses. *Atmospheric Chemistry and Physics*, *21*(8), 6079–6092. https://doi.org/10.5194/acp-21-6079-2021

Matsuno, T. (1971). A dynamical model of the stratospheric sudden warming. *Journal of the Atmospheric Sciences*, *28*(8), 1479–1494. https://doi.org/10.1175/1520-0469(1971)028<1479:ADMOTS>2.0.CO;2

Maury, P., Claud, C., Manzini, E., Hauchecorne, A., & Keckhut, P. (2016). Characteristics of stratospheric warming events during northern winter. *Journal of Geophysical Research: Atmospheres*, *121*(10), 5368–5380. https://doi.org/10.1002/2015JD024226

Mitchell, D. M., Gray, L. J., Anstey, J., Baldwin, M. P., & Charlton-Perez, A. J. (2013). The influence of stratospheric vortex displacements and splits on surface climate. *Journal of Climate*, *26*(8), 2668–2682. https://doi.org/10.1175/JCLI-D-12-00030.1

Newman, P. A., & Rosenfield, J. E. (1997). Stratospheric thermal damping times. *Geophysical Research Letters*, *24*(4), 433–436. https://doi.org/10.1029/96GL03720

North, G., Bell, T., Cahalan, R., & Moeng, F. (1982). Sampling errors in the estimation of empirical orthogonal functions. *Monthly Weather Review*, *110*(7), 699–706. https://doi.org/10.1175/1520-0493(1982)110<0699:SEITEO>2.0.CO;2

Pawson, S., & Kubitz, T. (1996). Climatology of planetary waves in the northern stratosphere. *Journal of Geophysical Research*, *101*(D12), 16987–16996. https://doi.org/10.1029/96JD01226

Rao, J., Ren, R., Chen, H., Yu, Y., & Zhou, Y. (2018). The stratospheric sudden warming event in February 2018 and its prediction by a climate system model. *Journal of Geophysical Research: Atmospheres*, *123*(23), 13332–13345. https://doi.org/10.1029/2018JD028908

Salby, M. L., & Callaghan, P. F. (2007). Influence of planetary wave activity on the stratospheric final warming and spring ozone. *Journal of Geophysical Research*, *112*(D20), D20111. https://doi.org/10.1029/2006JD007536

Scherhag, R. (1952). Die explosionsartigen stratospherener warmungen des spatwinters. *Berichte des Deutschen Wetterdienstes*, *38*, 51–63.

Simmons, A., Soci, C., Nicolas, J., Bell, B., Berrisford, P., Dragani, R., et al. (2020). Global stratospheric temperature bias and other stratospheric aspects of ERA5 and ERA5.1. ECMWF Technical Memoranda No. 859. https://doi.org/10.21957/rcxqfmg0

Thompson, D., & Wallace, J. (2001). Regional climate impacts of the Northern Hemisphere annular mode. *Science*, *293*(5527), 85–89. https://doi.org/10.1126/science.1058958

Vargin, P. N., Kostrykin, S. V., Rakushina, E. V., Volodin, E. M., & Pogoreltsev, A. I. (2020). Study of the variability of spring breakup dates and Arctic stratospheric polar vortex parameters from simulation and reanalysis data. *Izvestiya, Atmospheric and Oceanic Physics*, *56*(5), 458–469. https://doi.org/10.1134/S0001433820050114

Waugh, D., & Rong, P.-P. (2002). Interannual variability in the decay of lower stratospheric arctic vortices. *Journal of the Meteorological Society of Japan*, *80*(4B), 997–1012. https://doi.org/10.2151/jmsj.80.997